

Charmless $B_c \rightarrow VV$ decays in the QCD factorization approach

Qin Chang,^{1,2} Na Wang,^{1,2} Junfeng Sun,¹ and Lin Han¹

¹*Institute of Particle and Nuclear physics,*

Henan Normal University, Xinxiang 453007, China

²*Institute of Particle Physics and Key Laboratory of Quark and Lepton Physics (MOE),*

Central China Normal University, Wuhan 430079, China

Abstract

In this paper, we studied the charmless $B_c \rightarrow VV$ (V denotes the light ground SU(3) vector meson) decays within the framework of QCD factorization. In the evaluation, two different schemes for regulating the end-point divergence are adopted. One (scheme I) is to use parameterization model, which is usually employed in the QCD factorization approach; the other (scheme II) is based on the infrared finite gluon propagator of Cornwall prescription. It is found that, in the annihilation amplitudes, the end-point divergence appears only in the power-suppressed corrections related to the twist-3 distribution amplitudes of V -meson. The strength of annihilation amplitudes evaluated in scheme II is generally larger than the one in scheme I. Numerically, in the decay modes considered in this paper, the CKM-favored $B_c \rightarrow \rho^-\omega, K^{*-}K^{*0}$ decays have the relatively large branching fractions, $\sim \mathcal{O}(10^{-7})$, and hence are hopeful to be first observed by the future experiments. In addition, all of the decay modes are dominated by the longitudinal polarization state; numerically, $f_L(B_c \rightarrow VV) \gtrsim 99\%$.

Keywords: B_c meson; weak annihilation; QCD factorization

I. INTRODUCTION

The B_c^- meson is the only ground-pseudoscalar consisting of two heavy quarks with different flavor, namely a \bar{c} and a b quark. The difference of components flavors forbids B_c^- meson to annihilate into gluons or photons through strong interactions or electromagnetic interactions. Moreover, the B_c meson lies below the BD threshold. Therefore, it is considerably more stable than the charmonium or bottomonium states, and decays mainly through weak interaction. Since the b and c quarks can decay individually, the B_c meson has much richer decay modes than $B_{u,d,s}$ mesons [1], that could provide an ideal ground for studying the hadronic weak decays of heavy flavor quarks.

In the standard model (SM), the B_c weak decays can be divided into three categories: (1) the $b \rightarrow (c, u)W^-$ process with \bar{c} -quark as a spectator; (2) the $\bar{c} \rightarrow (\bar{s}, \bar{d})W^-$ process with b -quark as a spectator; (3) the pure weak annihilation $b\bar{c} \rightarrow W^-$ transition. Among the multitudinous B_c decay modes, the pure weak annihilation decay channels are expected to take 10% shares [2]. In the pure annihilation B_c decays, the major part comes from the “tree” annihilation processes induced by the CKM-favored $B_c^- \rightarrow s\bar{c}$ transition because of the sizable c -quark mass, while the charmless annihilation decays are relatively rare due to the power-suppression.

Experimentally, the production of B_c meson in hadron collisions implies the simultaneous production of $b\bar{b}$ and $c\bar{c}$ pairs, and therefore is relatively rarer than the other b mesons [3]. The heavy B_c meson was first observed by CDF collaboration from Run-I at Tevatron through the semileptonic decay mode $B_c^- \rightarrow J/\Psi l^- \bar{\nu}$ [4]. At the Large Hadron Collider (LHC) with a luminosity of about $\mathcal{L} = 10^{34} \text{cm}^{-2} \text{s}^{-1}$, around 5×10^{10} B_c events can be produced per year [5], and the measurements of the mass and lifetime of B_c meson have reached a very precise degree, for instance, $m_{B_c} = 6276.28 \pm 1.44 \pm 0.36 \text{ MeV}$ [6] and $\tau_{B_c} = 513.4 \pm 11.0 \pm 5.7 \text{ fs}$ [7] reported by the LHCb collaboration. Benefiting from the large production rate at LHC, a lot of B_c meson decays have been observed by LHCb collaboration, for instance: the $B_c^+ \rightarrow J/\Psi \pi^+ \pi^- \pi^+$ [8], $\Psi(2S) \pi^+$ [9], $J/\Psi D_s^{(*)}$ [6], $J/\Psi K^+$ [10], $J/\Psi K^+ K^- \pi^+$ [11] and $D^0 K^+$ [12] decay modes induced by the b quark decay, the first c quark decay mode $B_c^+ \rightarrow B_s^0 \pi^+$ [13] and the baryonic decay mode $B_c \rightarrow J/\Psi p \bar{p} \pi^+$ [14] *etc.*. In the near future, more B_c weak decays are expected to be measured at LHC with its high collision energy and high luminosity.

Theoretically, the weak decays of B_c meson are generally complicated because of its heavy-heavy nature and the participation of strong interaction, but they also provide opportunities to study the perturbative and nonperturbative QCD, final state interactions and heavy quarkonium properties, *etc.*. In the past years, some theoretical investigations have been carried out on the properties of B_c meson decays based on the QCD-inspired approaches, for instance, the operator product expansion [15, 16], the QCD sum rule [17, 18], the nonrelativistic QCD [19], the pQCD factorization approach [20–31], QCD factorization (QCDF) [32–34], the QCD relativistic potential models [35, 36] and the Bethe-Salpeter method [37, 38]. The two-body non-leptonic charmless B_c decay can occur only via the weak annihilation diagrams: the b and c quarks annihilate into a charged W^\pm boson that decays into a pair of a u and a d/s quark, which further hadronize into the two light mesons. Therefore, the charmless $B_c \rightarrow M_1 M_2$ ($M_{1,2}$ are the light mesons) decays are very suitable for probing the strength of annihilation contribution and exploiting the related mechanism, which are currently important issues in the B physics. Recently, the charmless $B_c \rightarrow VV$ decays are studied by using the $SU(3)$ flavor symmetry [33] and the pQCD approach [24]. In this article, we will revisit these decay modes by employing the QCDF approach [39, 40] to cope with the hadronic matrix elements.

In the theoretical framework based on the collinear factorization, the calculation of weak annihilation amplitude always suffers from the end-point singularities. In practice, there are two different phenomenological schemes proposed to deal with the end-point divergence in the QCDF approach. The scheme I is the parameterization method and has been widely employed in the previous works. In this scheme, the divergent integral is regulated by performing cutoff at $x = \Lambda_h/m_b$, where x is the momentum fraction of quark and $\Lambda_h \sim \Lambda_{\text{QCD}}$ is the parameter characterizing the point of cutoff (typically, $\Lambda_h = 0.5\text{GeV}$ [41, 42]) ; meanwhile, the integrals near end-point are treated as signs of infrared sensitive contributions, and parameterized by introducing the phenomenological parameters ρ_A and ϕ_A . Explicitly, the divergent integral is parameterized as $\int_0^1 dx/x \rightarrow X_A = \ln(m_b/\Lambda_h) (1 + \rho_A e^{i\phi_A})$ [41, 42]. As an alternative to the parameterization method, the end-point divergence could also be regulated by introducing an infrared finite dynamical gluon propagator [43–45], namely scheme II, which also has been successfully applied to the nonleptonic $B_{u,d,s}$ meson decays [46–50]. In this paper, above two regulation schemes are adopted respectively in our evaluation.

Our paper is organized as follows. In section II, after a brief review of the theoretical

framework for the two-body charmless hadronic B_c decays, the detailed calculation and discussion for the annihilation amplitudes in the QCDF are presented. Section III is devoted to the numerical results and discussion. Finally, we summarize in Sec. IV. The explicit expressions for the decay amplitudes and the relevant input parameters are collected in appendixes A and B, respectively.

II. THEORETICAL FRAMEWORK AND CALCULATION

A. The effective weak Hamiltonian and hadronic matrix element

The effective weak Hamiltonian responsible for the charmless $B_c^- \rightarrow V_1 V_2$ decays can be written as [51, 52]

$$\mathcal{H}_{\text{eff}} = \frac{G_F}{\sqrt{2}} V_{cb} V_{up}^* \left[C_1(\mu) Q_1 + C_2(\mu) Q_2 \right] + \text{h.c.}, \quad (1)$$

where G_F is the Fermi coupling constant, $V_{cb} V_{up}^*$ ($p = d, s$) is the product of CKM matrix elements [53], and $Q_{1,2}$ are local four-quark operators arisen from W -boson exchange and defined as

$$\begin{aligned} Q_1 &= [\bar{c}_\alpha \gamma^\mu (1 - \gamma_5) b_\alpha] [\bar{p}_\beta \gamma_\mu (1 - \gamma_5) u_\beta], \\ Q_2 &= [\bar{c}_\alpha \gamma^\mu (1 - \gamma_5) b_\beta] [\bar{p}_\beta \gamma_\mu (1 - \gamma_5) u_\alpha], \end{aligned} \quad (2)$$

with the color indices of α and β . The Wilson coefficient $C_i(\mu)$ in Eq. (1) describes the coupling strength for a given operator and summarizes the physical contributions above scale of μ . They are calculable perturbatively with the renormalization group improved perturbation theory [51, 52]. In addition, the $\overline{\text{MS}}$ renormalization scheme (RS) is employed in this work.

In order to obtain the decay amplitudes, the remaining works are to accurately calculate the hadronic matrix elements of local operators, $\langle VV | Q_i(\mu) | B_c \rangle$. In the QCDF, following the prescription proposed in Ref. [54], the hadronic matrix elements for the pure annihilation $B \rightarrow M_1 M_2$ decay can be written as the convolution integrals of the scattering kernel with the distribution amplitudes (DAs) of the participating mesons [39],

$$\langle M_1 M_2 | Q_i | \bar{B} \rangle = f_B f_{M_1} f_{M_2} \int dx dy dz \mathcal{T}_i^{II}(x, y, z) \varphi_{M_1}(x) \varphi_{M_2}(y) \varphi_B(z), \quad (3)$$

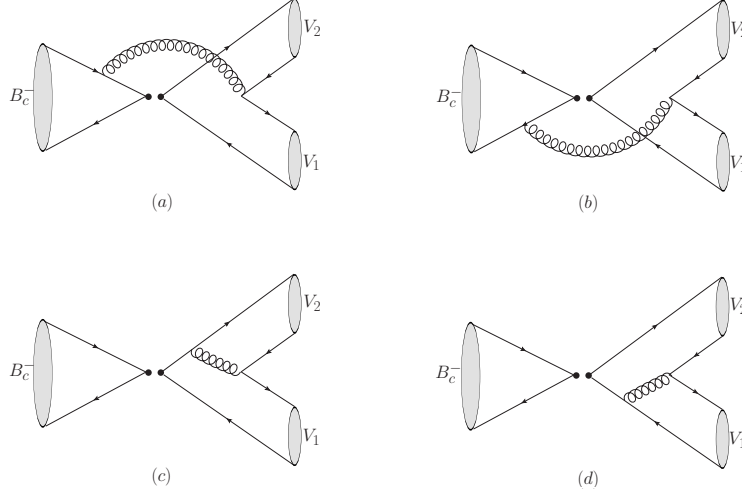


FIG. 1: The Feynman diagrams for the charmless $B_c^- \rightarrow V_1 V_2$ decays at the order of α_s .

where x, y, z are the momentum fractions; f_B and f_M are decay constants of the B and light mesons, respectively; and the kernel $\mathcal{T}_i^{II}(x, y, z)$ is hard-scattering functions.

For the $B_c \rightarrow VV$ decays, the kernel $\mathcal{T}_i^{II}(x, y, z)$ at the order of α_s can be obtained by calculating the Feynman diagrams shown in Fig. 1, in which Figs. (a), (b) and Figs. (c), (d) are non-factorizable and factorizable topologies, respectively. In these topologies, the contributions of factorizable diagrams, Figs. (c) and (d), cancel each other exactly in the QCDF approach due to the conservation of the vector current, partial conservation of axial-vector current, and the approximation that the twist-2 and twist-3 distribution amplitudes for the final states, V_1 and V_2 , have the same asymptotic expression. This situation is the same as the case of $B_{u,d,s} \rightarrow MM$ decays [41, 42, 55] and $B_c \rightarrow PP, PV$ decays [34]. In addition, because of the mismatch of the color indices, there is no contribution with insertion of the color-singlet operator, Q_1 , at the order of α_s .

Applying the QCDF formula, the decay amplitudes of $B_c \rightarrow VV$ decays can then be written as

$$\langle V_1 V_2 | \mathcal{H}_{\text{eff}} | B_c^- \rangle^\lambda \propto f_{B_c} f_{V_1} f_{V_2} b_2^\lambda(V_1, V_2), \quad (4)$$

where $\lambda = 0, \pm$ denote the helicities of the final-state vector mesons. The effective coefficient $b_2^\lambda(V_1, V_2)$ is defined as [41, 55]

$$b_2^\lambda(V_1, V_2) = \frac{C_F}{N_c^2} C_2 A_1^{i,\lambda}(V_1, V_2), \quad (5)$$

where $C_F = 4/3$ with $N_c = 3$. The superscript ‘ i ’ on $A_1^{i,\lambda}$ refers to the gluon emission from

the initial-state quarks, and the subscript ‘1’ refers to the $(V - A) \otimes (V - A)$ Dirac structure of the inserted four-quark operator Q_2 . The the explicit expressions of the building blocks, $A_1^{i,\lambda}$, will be given in the following subsections.

B. $A_1^{i,\lambda}(V_1, V_2)$ in scheme I

As aforementioned, the annihilation amplitude always suffers from the end-point divergence in the QCDF approach. Traditionally, the divergence is usually parameterized by introducing the complex parameters, $X_A = \ln(m_b/\Lambda_h) (1 + \rho_A e^{i\phi_A})$ [41], in which the phenomenological parameters ρ_A and ϕ_A reflect the strength and strong phase of the annihilation contributions. These parameters can only be obtained by fitting to the well-measured B decay modes, and then extended to predict the other decays [56–59]. Despite the fact that such a treatment is not entirely self-consistent, it is nevertheless useful for estimating the annihilation amplitude for particular final states, and has been wildly used in the theoretical calculation.

In this subsection, following such parameterization method, we adopt a similar way to estimate the charmless annihilation $B_c \rightarrow VV$ decays. Given that $m_{B_c} \simeq m_b + m_c$, the B_c meson can be approximated as a non-relativistic (NR) bound state that is dominated entirely by the two-particle Fock state built by a \bar{b} and a c quark. In such a NR limit, the soft components of the heavy-quark momentum can be neglected, and we can set the momentum of the valence quark to $p_b^\mu = m_b v^\mu$ and $p_c^\mu = m_c v^\mu$, where v^μ is the four-velocity of the B_c meson. This means that the light-cone momenta of the quarks are fixed according to their masses, and the distribution amplitude of the B_c meson then takes the peak form $\Phi_{B_c}(z) \propto \delta(z - m_c/m_{B_c})$ [20, 60, 61].

Following the convention adopted in Ref. [55] and using the peak form of $\Phi_{B_c}(z)$, we obtain the longitudinal component of annihilation amplitudes written as

$$A_1^{i,0}(V_1, V_2) = \pi\alpha_s(\mu) \int_0^1 dx dy \left\{ \Phi_{V_1}(x) \Phi_{V_2}(y) \left[\frac{1}{x[(x+\bar{y})z_b - x\bar{y} - i\epsilon]} - \frac{1}{\bar{y}[(x+\bar{y})z_c - x\bar{y} - i\epsilon]} \right] \right. \\ \left. - r_\chi^{V_1} r_\chi^{V_2} \Phi_{v_1}(x) \Phi_{v_2}(y) \left[\frac{x\bar{y} + (x+\bar{y} - 2x\bar{y})z_b}{x\bar{y}[(x+\bar{y})z_b - x\bar{y} - i\epsilon]} - \frac{x\bar{y} + (x+\bar{y} - 2x\bar{y})z_c}{x\bar{y}[(x+\bar{y})z_c - x\bar{y} - i\epsilon]} \right] \right\}; \quad (6)$$

and the transverse components are

$$\begin{aligned}
A_1^{i,-}(V_1, V_2) = & \pi\alpha_s(\mu) \frac{2m_1m_2}{m_{B_c}^2} \int_0^1 dx dy \left\{ \phi_{b1}(x) \phi_{b2}(y) \left[\frac{\bar{y} + z_b}{x\bar{y}[(x+\bar{y})z_b - x\bar{y} - i\epsilon]} \right. \right. \\
& + \frac{\bar{x}}{x^2[(x+\bar{y})z_b - x\bar{y} - i\epsilon]} - \frac{\bar{x}\bar{y}}{x[(x+\bar{y})z_b - x\bar{y} - i\epsilon]^2} \\
& \left. \left. - \frac{z_c}{x\bar{y}[(x+\bar{y})z_c - x\bar{y} - i\epsilon]} + \frac{\bar{x}}{[(x+\bar{y})z_c - x\bar{y} - i\epsilon]^2} \right] \right\}, \quad (7)
\end{aligned}$$

$$\begin{aligned}
A_1^{i,+}(V_1, V_2) = & \pi\alpha_s(\mu) \frac{2m_1m_2}{m_{B_c}^2} \int_0^1 dx dy \left\{ \phi_{a1}(x) \phi_{a2}(y) \left[\frac{z_b}{x\bar{y}[(x+\bar{y})z_b - x\bar{y} - i\epsilon]} \right. \right. \\
& - \frac{y}{[(x+\bar{y})z_b - x\bar{y} - i\epsilon]^2} - \frac{x + z_c}{x\bar{y}[(x+\bar{y})z_c - x\bar{y} - i\epsilon]} \\
& \left. \left. - \frac{y}{\bar{y}^2[(x+\bar{y})z_c - x\bar{y} - i\epsilon]} + \frac{xy}{\bar{y}[(x+\bar{y})z_c - x\bar{y} - i\epsilon]^2} \right] \right\}, \quad (8)
\end{aligned}$$

where x ($\bar{x} \equiv 1 - x$) and y ($\bar{y} \equiv 1 - y$) are the longitudinal momentum fractions of (anti-) quarks in V_1 and V_2 mesons, respectively; z_b and z_c denote the relative sizes of the b - and c -quark masses, $z_b = m_b/m_{B_c}$ and $z_c = m_c/m_{B_c}$; m_1 and m_2 are the masses of the final-state vector mesons; and the factor r_χ^V is defined as

$$r_\chi^V(\mu) = \frac{2m_V}{m_{B_c}} \frac{f_V^\perp(\mu)}{f_V} \quad (9)$$

where $m_V = m_1, m_2$; $f_V^\perp(\mu)$ is the scale-dependent transverse decay constant. Finally, we checked with the full results that in the limit $z_b \rightarrow 1$ and $z_c \rightarrow 0$ coincide with the results for $B_{u,d,s} \rightarrow VV$ decay in the heavy quark limit given by Eqs. (A.17) and (A.18) in Ref. [55]. In our following evaluations, the c -quark mass is reserved; in fact, we will show in the follows that the unnegligible c -quark mass plays an important role for eliminating the end-point divergency in the amplitudes of twist-2 part.

For the longitudinal amplitude, Eq. (6), only a few signs change in comparison with the known results for $B_c \rightarrow PP$ or PV decays [34]. Because $r_\chi^V(\mu)$ is suppressed by one power of Λ_{QCD}/m_b , the contributions related to the twist-3 DAs in Eq. (6) are small numerically. For the transverse amplitudes, from Eqs. (7) and (8), one can find that only the twist-3 terms of the light-cone projection operator contribute to them, and the transverse amplitudes are suppressed by two powers of Λ_{QCD}/m_b compared with the longitudinal amplitude. Therefore, the $B_c \rightarrow VV$ decay is expected to be dominated by longitudinal polarization.

Using the asymptotic expression for the distribution amplitudes of light vector meson [41, 55, 62]

$$\Phi_V(x) = \phi_\perp^V(x) = 6x(1-x), \quad \phi_a(x) = \phi_b(\bar{x}) = 3\bar{x}^2, \quad \Phi_v(x) = 3(x-\bar{x}), \quad (10)$$

the weak annihilation amplitudes of $B_{u,d,s} \rightarrow VV$ decays exhibit logarithmic and even linear infrared divergences [55], hence the analyses of these decays suffer from large uncertainties. It should be noted that the integral of the twist-2 part encounters the end-point divergence for $B_{u,d,s} \rightarrow VV$ decay, but is finite for $B_c \rightarrow VV$ decay due to the sizable c -quark mass which results in a complex contribution (it can be clearly seen from the second term proportional to $\Phi_{V_1} \Phi_{V_2}$ in Eq. (6)). Unfortunately, the logarithmic divergence exists still at twist-3 level for $B_c \rightarrow VV$ decay. Further considering the fact that all of the twist-3 contributions are power-suppressed by $(\Lambda_{\text{QCD}}/m_b)^2$ relative to the twist-2 part, we can expect that the prediction for $B_c \rightarrow VV$ decay in the framework of QCDF should be much more precise than $B_{u,d,s} \rightarrow VV$ decays.

In the numerical evaluation, one will encounter the physical-region singularity of the on mass-shell quark propagators and endpoint divergence of the gluon propagators in Eqs.(6)-(8). Here, we adopt the Cutkosky rule to deal with the singularities [63, 64]. For the divergence arising from the gluon propagator in the twist-3 part, because those terms are complex and hardly to be expressed as polynomial of X_A , we take the integral interval of $x, y \in [\Lambda_h/m_b, 1]$. In the following numerical evaluations of scheme I, we use $\Lambda_h = \Lambda_{\text{QCD}}^{\overline{\text{MS}}, n_f=3} = 332 \text{ MeV}$ [65], which is a little smaller than the typical choice, $\Lambda_h = 500 \text{ MeV}$. The effect of Λ_h will be discussed briefly in the follows.

The numerical results for the building blocks $A_1^{i,\lambda}$ with the default inputs summarized in Appendix B are

$$A_1^{i,0}(V_1, V_2) = \pi [(-5.64 - 6.22i) - r_\chi^{V_1} r_\chi^{V_2} (-1.83 - 2.94i)], \quad (11)$$

$$A_1^{i,-}(V_1, V_2) = \pi \frac{2m_1 m_2}{m_{B_c}^2} (3.32 + 4.57i), \quad (12)$$

$$A_1^{i,+}(V_1, V_2) = \pi \frac{2m_1 m_2}{m_{B_c}^2} (-10.50 - 1.49i). \quad (13)$$

As we expected, the transverse amplitudes and the twist-3 term in the longitudinal amplitude are numerically small due to the power-suppression factor $m_1 m_2 / m_{B_c}^2 \sim \mathcal{O}(10^{-2})$, and therefore, the amplitude of $B_c \rightarrow VV$ decay is dominated by the contribution of twist-2 term

in $A_1^{i,0}$. Further considering the fact that the value of Λ_h only affects the integral of twist-3 part, we can conclude that the effect of Λ_h on the total amplitude is small. For instance, using $\Lambda_h = 0.2$ and 0.5 GeV, respectively, we obtain

$$A_1^{i,0}(\rho^- \omega) = -17.58 - 19.28i \quad \text{vs.} \quad -17.51 - 19.28i \quad (14)$$

for $B_c \rightarrow \rho^- \omega$ decay. It can be clearly seen that the theoretical uncertainty induced by Λ_h is at the level of $\lesssim 1\%$.

C. $A_1^{i,\lambda}(V_1, V_2)$ in scheme II

In this subsection, we shall quote the infrared finite gluon propagator to regulate the divergences in the annihilation amplitudes. The infrared finite (IR) dynamical gluon propagator, which is shown to be not divergent as fast as $1/q^2$, has been successfully applied to various hadronic $B_{u,d,s}$ decays [46–50]. It should be noted that an IR finite gluon propagator typically leads to a freezing coupling $\alpha_s(0)$ [66, 67] (one may refer to Ref. [66] for detail). The infrared finite behavior is not only obtained from solving the well-known Schwinger-Dyson equation [43, 68], but also supported by recent lattice simulations [69, 70] and the studies based on the light-front holographic (AdS₅) QCD [71]. In addition, a freezing α_s is also used as a regulator in Ref. [72] as we do in this scheme.

In the practice, we adopt the Cornwall's prescription for the IR finite gluon propagator [43],

$$D(q^2) = \frac{1}{q^2 - M_g^2(q^2) + i\epsilon}, \quad (15)$$

where q^2 denotes the gluon momentum squared. The corresponding coupling constant including the quark loops correction reads [43–45]

$$\alpha_s^C(q^2) = \frac{12\pi}{33 \ln \left[\frac{q^2 + \epsilon M_g^2(q^2)}{\Lambda_C^2} \right] - 2n_f \ln \left[\frac{q^2 + \epsilon M^2}{\Lambda_C^2} \right]}, \quad (16)$$

where Λ_C is the QCD scale, $\epsilon = 4.8$, $M = 0.42$ GeV is identified with the string tension [45, 66], and n_f is the number of active quark flavors at a given scale. The dynamical gluon mass $M_g^2(q^2)$ is given by [43–45]

$$M_g^2(q^2) = m_g^2 \left[\frac{\ln(\frac{q^2 + 4m_g^2}{\Lambda_C^2})}{\ln(\frac{4m_g^2}{\Lambda_C^2})} \right]^{-\frac{12}{11}}, \quad (17)$$

where m_g is the effective gluon mass scale with a typical value $m_g = 0.5 \pm 0.2$ GeV [43]. The value of m_g can be determined from the phenomenological information. For instance, a good description of the experimental pion and kaon form factors is obtained for $m_g = 0.54$ GeV [73, 74]; while, the authors of Ref. [75] find that $m_g = 0.70$ GeV describes the pion form factor data well; the value $m_g = 0.44$ GeV is suggested to analyze the photon-to-pion transition form factor and $\gamma\gamma \rightarrow \pi^+\pi^-$ decay [76]; the similar values are obtained by fitting to the experimental data of non-leptonic B decays, $m_g = 0.5 \pm 0.05$ GeV for $B_{u,d}$ decays [48] and $m_g = 0.48 \pm 0.02$ GeV for B_s decays [49]. One may refer to Ref. [66] and literatures therein for details for this part. In this work, we take a conservative choice $m_g = 0.5 \pm 0.2$ GeV [43].

The typical value of Λ_C is 0.26 ± 0.05 GeV [43–45, 66], which is usually used for, for instance, studying the IR behavior of strong coupling. For the annihilation B_c decays, the range of momentum squared of gluon is very large; therefore, the values of Λ_C , as well as n_f , should be non-universal in different q^2 bins in principle. In addition, the large momentum-transfer dependence of the coupling α_s is generally specified by perturbative QCD (PQCD) and its renormalization group equation. Thus, in order to obtain the values of Λ_C , we try to match α_s^C to α_s^{PQCD} at $q^2 = m_b^2, m_c^2$ and 1 GeV^2 with $n_f = 5, 4$ and 3 , respectively.

In the matching procedure, the world averages of $\Lambda_{\text{PQCD}}^{(n_f)}$ [65] listed in Table I are used; in addition, the approximate analytical expression for α_s^{PQCD} up to order β_3 [77] in the $\overline{\text{MS}}$ RS is employed. Using the matching condition $\alpha_s^C = \alpha_s^{\text{PQCD}}$, we finally obtain ^a

$$\Lambda_C^{n_f=3,4,5}[\text{GeV}] = 0.35, 0.22, 0.10, \quad (18)$$

which are in agreement with the typical value 0.26 ± 0.05 GeV except at large $q^2 > m_b^2$ with $n_f = 5$. Such values will be used in the intervals $q^2 < m_c^2$, $m_c^2 < q^2 < m_b^2$ and $q^2 > m_b^2$ ^b, respectively, in our following evaluations.

In Table I, we summarize the results of α_s at different matching point of q^2 . In addition, in order to further test the values of Λ_C given above, the values of α_s at large $q^2 = m_Z^2$

^a These values can be treated as the “effective” scale absorbing the higher order loops “corrections” because the 4-loops result for α_s^{PQCD} is used in the matching procedure (In other words, we require α_s^C with a proper Λ_C to reproduce the 4-loops α_s^{PQCD} in $\overline{\text{MS}}$ RS at interval of $q^2 > 1 \text{ GeV}^2$).

^b In the QCDF, the pole mass of the light quarks, u, d and s , are taken to be zero in the heavy quark limit, therefore the case of $n_f = 2$ is not considered. The effect of such approximation is trivial numerically because it corresponds to a very narrow integral space.

TABLE I: The results of α_s with the scales Λ at different q^2 . The uncertainties in the last row for $\alpha_s^C(q^2)$ is induced by $m_g = 0.5 \pm 0.2$ GeV. See the text for the further explanation.

| $q^2[\text{GeV}]$ | 0 | 1 | m_c^2 | m_b^2 | m_Z^2 |
|--|---------------------------|---------------------------|---------------------------|---------------------------|---------------------------|
| n_f | 3 | 3 | 4 | 5 | 5 |
| $\Lambda_{\text{PQCD}}[\text{GeV}]$ [65] | — | 0.332 | 0.292 | 0.210 | 0.210 |
| $\Lambda_C[\text{GeV}]$ | 0.35 | 0.35 | 0.22 | 0.10 | 0.10 |
| $\alpha_s^{\text{PQCD}}(q^2)$ | — | 0.584 | 0.354 | 0.218 | 0.118 |
| $\alpha_s^C(q^2)$ | $0.644_{-0.177}^{+0.877}$ | $0.532_{-0.096}^{+0.147}$ | $0.357_{-0.027}^{+0.022}$ | $0.212_{-0.002}^{+0.001}$ | $0.120_{-0.000}^{+0.000}$ |

and freezing point $q^2 = 0$ are also listed in the Table I. It can be found that: (i) Using the $\Lambda_C = 0.1$ GeV fitted at $q^2 = m_b^2$, our prediction $\alpha_s^C(m_Z^2) = 0.120$ is in agreement with the $\alpha_s^{\text{PQCD}}(m_Z^2)$ and the experimental data 0.1182 [65]. Moreover, the uncertainty induced by the $m_g = 0.5 \pm 0.2$ GeV vanishes at $q^2 = m_Z^2$, but is very large at small q^2 region. (ii) Our prediction for the freezing value, $\alpha_s^C(0) = 0.644_{-0.177}^{+0.877}$, is also in agreement with, for instance, $\alpha_s^{\text{LFH}}(0) = 1.22 \pm 0.04 \pm 0.11 \pm 0.09$ [71] obtained in the framework of the light-front holographic QCD and $\overline{\text{MS}}$ RS, within the theoretical uncertainties.

Using above formulae and the same convention as scheme I, we obtain the annihilation amplitudes,

$$\begin{aligned}
A_1^{i,0}(V_1, V_2) = \pi \int_0^1 dx dy \alpha_s^C(q^2) \left\{ \Phi_{V_1}(x) \Phi_{V_2}(y) \left[\frac{\bar{y}}{(x\bar{y} - \omega^2(q^2) + i\epsilon)[(x + \bar{y})z_b - x\bar{y} - i\epsilon]} \right. \right. \\
\left. \left. - \frac{x}{(x\bar{y} - \omega^2(q^2) + i\epsilon)[(x + \bar{y})z_c - x\bar{y} - i\epsilon]} \right] \right. \\
\left. - r_\chi^{V_1} r_\chi^{V_2} \Phi_{v_1}(x) \Phi_{v_2}(y) \left[\frac{x\bar{y} + (x + \bar{y} - 2x\bar{y})z_b}{(x\bar{y} - \omega^2(q^2) + i\epsilon)[(x + \bar{y})z_b - x\bar{y} - i\epsilon]} \right. \right. \\
\left. \left. - \frac{x\bar{y} + (x + \bar{y} - 2x\bar{y})z_c}{(x\bar{y} - \omega^2(q^2) + i\epsilon)[(x + \bar{y})z_c - x\bar{y} - i\epsilon]} \right] \right\}, \quad (19)
\end{aligned}$$

$$\begin{aligned}
A_1^{i,-}(V_1, V_2) = \pi \frac{2m_1 m_2}{m_{B_c}^2} \int_0^1 dx dy \alpha_s^C(q^2) \phi_{b1}(x) \phi_{b2}(y) \\
\left[\left(\frac{\bar{y} + z_b}{(x\bar{y} - \omega^2(q^2) + i\epsilon)[(x + \bar{y})z_b - x\bar{y} - i\epsilon]} + \frac{\bar{x} - z_c}{(x\bar{y} - \omega^2(q^2) + i\epsilon)[(x + \bar{y})z_c - x\bar{y} - i\epsilon]} \right) \right]
\end{aligned}$$

$$\begin{aligned}
& + \left(\frac{\bar{x}\bar{y}^2}{(x\bar{y} - \omega^2(q^2) + i\epsilon)^2[(x + \bar{y})z_b - x\bar{y} - i\epsilon]} - \frac{\bar{x}\bar{y}^2}{(x\bar{y} - \omega^2(q^2) + i\epsilon)[(x + \bar{y})z_b - x\bar{y} - i\epsilon]^2} \right) \\
& - \left(\frac{x\bar{x}\bar{y}}{(x\bar{y} - \omega^2(q^2) + i\epsilon)^2[(x + \bar{y})z_c - x\bar{y} - i\epsilon]} - \frac{x\bar{x}\bar{y}}{(x\bar{y} - \omega^2(q^2) + i\epsilon)[(x + \bar{y})z_c - x\bar{y} - i\epsilon]^2} \right) \Big],
\end{aligned} \tag{20}$$

$$\begin{aligned}
A_1^{i,+}(V_1, V_2) &= \pi \frac{2m_1 m_2}{m_{B_c}^2} \int_0^1 dx dy \alpha_s^C(q^2) \phi_{a1}(x) \phi_{a2}(y) \\
& \left[\left(\frac{z_b - y}{(x\bar{y} - \omega^2(q^2) + i\epsilon)[(x + \bar{y})z_b - x\bar{y} - i\epsilon]} - \frac{x + z_c}{(x\bar{y} - \omega^2(q^2) + i\epsilon)[(x + \bar{y})z_c - x\bar{y} - i\epsilon]} \right) \right. \\
& + \left(\frac{xy\bar{y}}{(x\bar{y} - \omega^2(q^2) + i\epsilon)^2[(x + \bar{y})z_b - x\bar{y} - i\epsilon]} - \frac{xy\bar{y}}{(x\bar{y} - \omega^2(q^2) + i\epsilon)[(x + \bar{y})z_b - x\bar{y} - i\epsilon]^2} \right) \\
& \left. - \left(\frac{x^2 y}{(x\bar{y} - \omega^2(q^2) + i\epsilon)^2[(x + \bar{y})z_c - x\bar{y} - i\epsilon]} - \frac{x^2 y}{(x\bar{y} - \omega^2(q^2) + i\epsilon)[(x + \bar{y})z_c - x\bar{y} - i\epsilon]^2} \right) \right],
\end{aligned} \tag{21}$$

where, $\omega^2(q^2) = M_g^2(q^2)/m_{B_c}^2$ with $q^2 \simeq x\bar{y}m_{B_c}^2$ the time-like gluon momentum square. Here, we would like to clarify that the IR finite gluon propagator given by Eq. (15) is used for evaluating both twist-3 and twist-2 contributions for consistence, although it is not essential for the latter from the viewpoint of regulating end-point divergence (the integral of twist-2 part is finite as has been mentioned in the last subsection). Again we checked that the results for $B_{u,d,s} \rightarrow VV$ decay with IR finite gluon propagator, which have been calculated in Ref. [49], can be recovered from above formulae by taking the limits $z_b \rightarrow 1$ and $z_c \rightarrow 0$.

From Eqs. (19), (20) and (21), it is found that the singularities of the gluon propagators are moved from end-point into integral intervals by using the infrared finite form of the gluon propagator. Using $m_g = 0.5$ GeV, we obtain the numerical results for the building blocks $A_1^{i,\lambda}(V, V)$ in scheme II that

$$A_1^{i,0}(V_1, V_2) = \pi [(-10.33 - 5.21i) - r_\chi^{V_1} r_\chi^{V_2} (-1.40 - 8.75i)], \tag{22}$$

$$A_1^{i,-}(V_1, V_2) = \pi \frac{2m_1 m_2}{m_{B_c}^2} (16.82 - 2.13i), \tag{23}$$

$$A_1^{i,+}(V_1, V_2) = \pi \frac{2m_1 m_2}{m_{B_c}^2} (-17.33 + 8.18i). \tag{24}$$

Comparing with the results in scheme I, we find that the annihilation contributions are enhanced when we adopt the infrared finite gluon propagator.

It is known that the form of IR finite gluon propagator, Eqs. (16) and (17), is model-dependent. In order to estimate the model-dependence of scheme II, we would like to reevaluate the annihilation amplitude by using Aguilar-Papavassiliou (AP)'s prescription [78] instead of Cornwall's solution. The relevant formulae and inputs are collected in Appendix C. For simplicity, we take $A_1^{i,0}(\rho^-\omega)$ as an example. The result evaluated by using Cornwall's solution with $m_g = 0.5 \pm 0.2 \text{ GeV}$ are also shown in the follows for convenience of comparison. Numerically, we obtain

$$|A_1^{i,0}(\rho^-\omega)| = 32.56 \text{ (AP)} \quad \text{vs.} \quad 36.36_{-4.47}^{+6.73} \text{ (Cornwall)}. \quad (25)$$

It can be clearly seen that these results are consistent with each other within the uncertainties of m_g (*i.e.*, the possible model-dependence of scheme II could be accommodate by using a conservative input, $m_g = 0.5 \pm 0.2 \text{ GeV}$).

III. NUMERICAL RESULTS AND DISCUSSIONS

Using the building blocks given in the last section, we summarize the polarization-dependent decay amplitudes $\mathcal{A}_\lambda(B_c^- \rightarrow V_1 V_2)$ in the Appendix A. The branching ratios for charmless $B_c^- \rightarrow V_1 V_2$ decays in the rest frame of B_c^- meson can be written as

$$\mathcal{B}(B_c^- \rightarrow V_1 V_2) = \frac{\tau_{B_c}}{8\pi} \frac{|\vec{p}|}{m_{B_c}^2} \sum_\lambda |\mathcal{A}_\lambda(B_c^- \rightarrow V_1 V_2)|^2, \quad (26)$$

where $\tau_{B_c} = 0.507 \text{ ps}$ [65] is the lifetime of B_c -meson, and $|\vec{p}|$ is the center-of-mass momentum of either of the two outgoing mesons,

$$|\vec{p}| = \frac{\sqrt{[m_{B_c}^2 - (m_{V_1} + m_{V_2})^2][m_{B_c}^2 - (m_{V_1} - m_{V_2})^2]}}{2m_{B_c}}. \quad (27)$$

Besides of the branching fraction, the polarization fractions defined as

$$f_{L,\parallel,\perp} = \frac{|\mathcal{A}_{0,\parallel,\perp}|^2}{|\mathcal{A}_0|^2 + |\mathcal{A}_\parallel|^2 + |\mathcal{A}_\perp|^2} \quad (28)$$

are also very important observable, where \mathcal{A}_\parallel and \mathcal{A}_\perp are parallel and perpendicular amplitudes and could be easily gotten through $\mathcal{A}_{\parallel,\perp} = (\mathcal{A}_- \pm \mathcal{A}_+)/\sqrt{2}$. In addition, the CP-violating asymmetries for all of the decay modes considered in this paper are absent.

With the theoretical formulae given above and the input parameters collected in Appendix B, we proceed to present the numerical results for the CP-averaged branching ratios

TABLE II: The CP-averaged branching ratios (in units of 10^{-8}) of $B_c \rightarrow VV$ decays based on the two regulation schemes. The theoretical errors correspond to the uncertainties induced by “CKM”, “hadronic”, “scale”, and “ m_g ”. The pQCD predictions [24] are also listed in the last column.

| Decay modes | Cases | Scheme I | Scheme II | pQCD |
|---|------------------|---|--|-----------------------|
| $B_c^- \rightarrow \rho^- \rho^0$ | $ \Delta S = 0$ | 0 | 0 | 0 |
| $B_c^- \rightarrow \rho^- \omega$ | $ \Delta S = 0$ | $16.1^{+0.8+2.9+50.3}_{-1.1-2.5-12.0}$ | $30.6^{+1.6+5.6+41.7+14.3}_{-2.1-4.7-18.7-6.1}$ | 106^{+32+21}_{-2-2} |
| $B_c^- \rightarrow K^{*-} K^{*0}$ | $ \Delta S = 0$ | $9.21^{+0.47+1.39+28.79}_{-0.63-1.16-6.86}$ | $17.5^{+0.9+2.7+23.9+8.8}_{-1.2-2.2-10.7-3.5}$ | 100^{+6+81}_{-4-48} |
| $B_c^- \rightarrow K^{*-} \rho^0$ | $ \Delta S = 1$ | $0.26^{+0.01+0.04+0.82}_{-0.02-0.03-0.19}$ | $0.50^{+0.03+0.07+0.68+0.24}_{-0.04-0.06-0.31-0.10}$ | 3^{+0+1}_{-0-1} |
| $B_c^- \rightarrow \bar{K}^{*0} \rho^-$ | $ \Delta S = 1$ | $0.53^{+0.02+0.07+1.64}_{-0.04-0.07-0.40}$ | $1.00^{+0.05+0.14+1.36+0.48}_{-0.07-0.12-0.61-0.20}$ | 6^{+0+2}_{-0-1} |
| $B_c^- \rightarrow K^{*-} \omega$ | $ \Delta S = 1$ | $0.20^{+0.02+0.02+0.64}_{-0.01-0.03-0.15}$ | $0.39^{+0.02+0.07+0.53+0.18}_{-0.03-0.07-0.24-0.08}$ | 3^{+0+0}_{-0-2} |
| $B_c^- \rightarrow \phi K^{*-}$ | $ \Delta S = 1$ | $0.58^{+0.04+0.06+1.83}_{-0.04-0.05-0.43}$ | $1.11^{+0.05+0.12+1.51+0.57}_{-0.08-0.10-0.68-0.22}$ | 5^{+0+1}_{-1-3} |

of $B_c \rightarrow VV$ decays. In our calculation, the default value of renormalization scale is set at $\mu = m_{B_c}/2$, which is approximately the averaged virtuality of the time-like gluon propagated in the annihilation diagrams. The numerical results based on the two schemes for regulating the end-point divergence are collected in Table II. In this table, we present the “default results” along with the detailed errors estimated with different theoretical uncertainties of inputs. The first error refers to the variation of the CKM parameters (named as “CKM”); the second error corresponds to the quark masses and decay constants (named as “hadronic”); the third error originates from the variation of the renormalization scale μ (named as “scale”); the last error in scheme II reflects the uncertainty of the effective gluon mass m_g (named as “ m_g ”). For comparison, predictions of the pQCD factorization approach [24] are also listed in the last column of Table II (the $\overline{\text{MS}}$ RS is used in the pQCD calculation, see Refs. [24, 79] for detail).

Based on the results collected in Table II, we have the following observations and remarks:

- From the decay amplitudes summarized in the Appendix A, it can be found that the CKM matrix elements and Wilson coefficients are the key factors to determine the size of the amplitude. The strangeness-changing ($|\Delta S| = 1$) processes are CKM-suppressed relative to the strangeness-conserving ($|\Delta S| = 0$) processes due to the hierarchy of the

CKM matrix elements, $|V_{ud}/V_{us}|^2 \sim 19$. As a result, the branching ratios of $|\Delta S| = 0$ decay channels are generally much larger than those of $|\Delta S| = 1$ ones by about an order of magnitude.

- Because the contributions from $u\bar{u}$ and $d\bar{d}$ components of the ρ^0 meson, $|\rho^0\rangle = (|u\bar{u}\rangle - |d\bar{d}\rangle)/\sqrt{2}$, cancel with each other exactly, the branching ratio of $B_c^- \rightarrow \rho^- \rho^0$ decay is zero. On the other hand, for $B_c^- \rightarrow \rho^- \omega$ decay, the interference between the two flavor components $u\bar{u}$ and $d\bar{d}$ of the ω meson is constructive due to $|\omega\rangle = (|u\bar{u}\rangle + |d\bar{d}\rangle)/\sqrt{2}$, which results in a large branching ratio.
- Among the charmless $B_c \rightarrow VV$ decays considered in this work, the CKM-favored $B_c^- \rightarrow \rho^- \omega$, $K^{*-} K^{*0}$ decay modes have relatively large branching ratios being around $\mathcal{O}(10^{-7})$. It is also found that $B_c^- \rightarrow \rho^- \omega$ decay has the the largest branching ratio, $\sim 30.6 \times 10^{-8}$, and hence will possibly be observed earlier at LHC and SuperKEKB.
- In the limit of the $SU(3)$ flavor-symmetry, the relation

$$\mathcal{A}(B_c^- \rightarrow \bar{K}^{*0} \rho^-) = \sqrt{2} \mathcal{A}(B_c^- \rightarrow K^{*-} \rho^0) = \hat{\lambda} \mathcal{A}(B_c^- \rightarrow K^{*-} K^{*0}), \quad (29)$$

with the Cabibbo-suppressing factor $\hat{\lambda} = V_{us}/V_{ud}$ is expected. In our calculation, we take the asymptotic expressions for the distribution amplitudes of V mesons, and the flavor-asymmetry effect arises only from the chiral enhancement parameter r_χ^V and decay constants. Therefore, the $SU(3)$ breaking effect turns out to be relatively small, and above relation still holds approximately in both scheme I and II which can be seen from Table II.

- In scheme II, using the central values of input parameters summarized in Appendix B and the AP's prescription [78] given in Appendix C instead of Eqs. (16) and (17), we have calculated the branching ratios of the $|\Delta S| = 0$ processes, and obtain

$$\mathcal{B}(B_c^- \rightarrow \rho^- \omega) = 25.0 \times 10^{-8}, \quad \mathcal{B}(B_c^- \rightarrow K^{*-} K^{*0}) = 14.5 \times 10^{-8}. \quad (30)$$

Comparing with corresponding results in Table II, one can find that such results are in agreement with the ones obtained by using Cornwall's formulae, Eqs. (16) and (17), within the theoretical uncertainties of $m_g = 0.5 \pm 0.2 \text{ GeV}$.

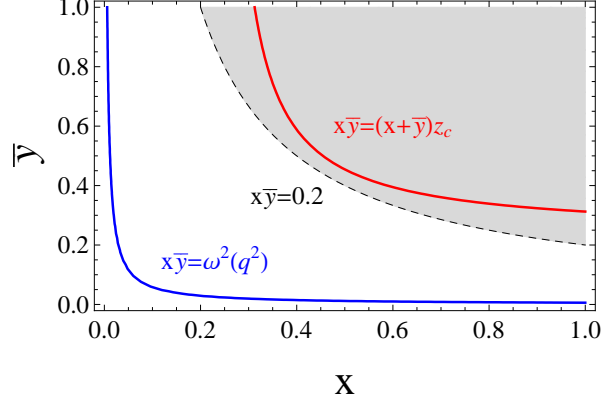


FIG. 2: The singularities in the integrals induced by the c -quark mass (red line) and the dynamical gluon mass (blue line). The dashed line and shaded region correspond to $x\bar{y} = 0.2$ and $0.2 \leq x\bar{y} \leq 1$, respectively (see text for explanation).

- As mentioned in the last section, the annihilation contributions are enhanced when we adopt the IR finite gluon propagator. It is mainly caused by that: (i) In scheme I, the strong coupling in the amplitude is determined by the scale μ with the default value $m_{B_c}/2$; while, $\alpha_s(q^2)$ in scheme II is determined by Eq. (16), and relatively larger than the one in scheme I at low q^2 region. (ii) It have been found that the singularities in the integral interval can significantly affect the numerical results of the integrals in the annihilation amplitudes, for instance, Ref [48]. In scheme I, the singularities $x\bar{y} = (x + \bar{y})z_c$ is induced by the sizable c -quark mass; while, in scheme II, besides $x\bar{y} = (x + \bar{y})z_c$, additional singularities $x\bar{y} = \omega^2(q^2)$ induced by effective gluon mass enter into the integral interval (the singularities are shown in Fig. 2). As a result, the branching ratios in scheme II are generally larger than the ones in scheme I, but they are still in agreement within the large theoretical uncertainties.

In fact, schemes I and II result in similar annihilation contributions at large q^2 region. In order to clearly show that, we take the integral interval $0.2 \leq x\bar{y} \leq 1$, which is far from the the singularities $x\bar{y} = \omega^2(q^2)$ as Fig. 2 shows; and take the amplitude of twist-2 part in $A_1^{i,0}$ as an example, which plays a dominative role in the annihilation amplitudes. Then, using the central values of the other inputs, we obtain

$$|A_1^{i,0}(\text{twist-2})|_{0.2 \leq x\bar{y} \leq 1} = 20.1 \text{ (scheme I) vs. } 22.9 \text{ (scheme II)}, \quad (31)$$

which are similar to each other, and therefore, confirm our analyses given above.

- From Table II, we find that our predictions (central value) are relatively smaller than the ones in the pQCD factorization approach [24]. The different choices of the renormalization scale and strategies for coping with the end-point contributions may be the main reasons leading to these discrepancies.

For the $B_c^- \rightarrow \bar{K}^{0*}\rho^-$ and $K^{*-}\rho^0$ decays induced by the strangeness-changing ($|\Delta S| = 1$) transition, the relation

$$\mathcal{B}(B_c^- \rightarrow \bar{K}^{0*}\rho^-) = 2 \times \mathcal{B}(B_c^- \rightarrow K^{*-}\rho^0) \quad (32)$$

is expected by $SU(3)$ flavor-symmetry as Eq. (29) shows, and also can be clearly seen from Eqs. (A4) and (A5). It can be found from Table II that such relation is favored by the predictions of this work and pQCD approach. For the strangeness-conserving ($|\Delta S| = 0$) processes, the amplitudes, Eqs. (A2) and (A3), imply a rough relation similar to Eq. (32), $\mathcal{B}(B_c^- \rightarrow \rho^-\omega) \sim 2 \times \mathcal{B}(B_c^- \rightarrow K^{*-}K^{*0})$. It is satisfied by our results but disfavored by pQCD, which can be seen from Table II.

The heavy flavor experiments at LHC and SuperKEKB/Belle-II in the future are expected to exhibit a clear picture for the annihilation contributions.

- As we have mentioned, because only the twist-3 terms of the light-cone projector for the final-state V mesons contribute to the transverse amplitudes, one can find from Eqs. (6-8) and (19-21) that $A_1^{i,\pm}$ are suppressed by two powers of Λ_{QCD}/m_{B_c} compared with $A_1^{i,0}$. As a result, all of the $B_c \rightarrow VV$ decays are dominated by longitudinal polarization. Numerical, we obtain $f_L(B_c \rightarrow VV) \gtrsim 99\%$, which is a little larger than the pQCD prediction $f_L(B_c \rightarrow VV) \sim [86, 95]\%$ [24] and will be tested by the future measurements.

IV. SUMMARY

In this paper, we have studied the nonleptonic charmless $B_c \rightarrow VV$ decays within the framework of QCD factorization. These decay modes can occur only via the weak annihilation diagram, which involves only a tree operator, Q_2 , at the order of α_s , and therefore, they will provide an important testing ground for the magnitude of annihilation contribution and the underlying mechanism.

It is found that the transverse amplitudes and the twist-3 part of longitudinal amplitude are power-suppressed by $(\Lambda_{QCD}/m_{B_c})^2$ relative to the main contribution (the twist-2 part of longitudinal amplitude), and are small numerically. For the main contribution, the problem of end-point divergence, which appeared in the $B_{u,d,s} \rightarrow MM$ decays, vanishes in the $B_c \rightarrow VV$ decays due to the sizable c -quark mass. However, it still exists in the power-suppressed corrections. In order to regulate the end-point divergence, we have employed two different schemes based on the parameterization and the infrared finite gluon propagator with a dynamical gluon mass, respectively. Our predictions for the branching fractions of $B_c \rightarrow VV$ decays are collected in Table II, in which the $B_c^- \rightarrow \rho^- \omega$ and $K^{*-} K^{*0}$ decays have relatively large branching ratio, $\sim 10^{-7}$, and hence have the best potential for the detection. In addition, the longitudinal polarization fractions are expected at the level of 99% for all of the $B_c \rightarrow VV$ decays. Then, some phenomenological analyses and discussions are made. All of the findings in this paper are waiting for the experimental test at LHC and SuperKEKB/Belle-II in the future.

Appendix A: Decay amplitudes of $B_c \rightarrow VV$ decays

Starting with Eq. (4) and adopting the standard phase convention for the flavor wavefunctions of light and heavy mesons [41, 55, 80], one can easily write down the decay amplitude for a given decay mode. There are seven charmless $B_c \rightarrow VV$ decays with the corresponding amplitude given, respectively, as (the exact isospin symmetry is assumed):

$$\mathcal{A}^\lambda(B_c^- \rightarrow \rho^- \rho^0) = \frac{G_F}{2} V_{cb} V_{ud}^* f_{B_c} f_{\rho^-} f_{\rho^0} [b_2^\lambda(\rho^0, \rho^-) - b_2^\lambda(\rho^-, \rho^0)] = 0, \quad (\text{A1})$$

$$\mathcal{A}^\lambda(B_c^- \rightarrow \rho^- \omega) = \frac{G_F}{2} V_{cb} V_{ud}^* f_{B_c} f_{\rho^-} f_\omega [b_2^\lambda(\omega, \rho^-) + b_2^\lambda(\rho^-, \omega)], \quad (\text{A2})$$

$$\mathcal{A}^\lambda(B_c^- \rightarrow K^{*-} K^{*0}) = \frac{G_F}{\sqrt{2}} V_{cb} V_{ud}^* f_{B_c} f_{K^{*-}} f_{K^{*0}} b_2^\lambda(K^{*-}, K^{*0}), \quad (\text{A3})$$

$$\mathcal{A}^\lambda(B_c^- \rightarrow K^{*-} \rho^0) = \frac{G_F}{2} V_{cb} V_{us}^* f_{B_c} f_{K^{*-}} f_{\rho^0} b_2^\lambda(\rho^0, K^{*-}), \quad (\text{A4})$$

$$\mathcal{A}^\lambda(B_c^- \rightarrow \bar{K}^{0*} \rho^-) = \frac{G_F}{\sqrt{2}} V_{cb} V_{us}^* f_{B_c} f_{\bar{K}^{0*}} f_{\rho^-} b_2^\lambda(\rho^-, \bar{K}^{0*}), \quad (\text{A5})$$

$$\mathcal{A}^\lambda(B_c^- \rightarrow K^{*-} \omega) = \frac{G_F}{2} V_{cb} V_{us}^* f_{B_c} f_{K^{*-}} f_\omega b_2^\lambda(\omega, K^{*-}), \quad (\text{A6})$$

$$\mathcal{A}^\lambda(B_c^- \rightarrow \phi K^{*-}) = \frac{G_F}{\sqrt{2}} V_{cb} V_{us}^* f_{B_c} f_\phi f_{K^{*-}} b_2^\lambda(K^{*-}, \phi). \quad (\text{A7})$$

Appendix B: Input parameters

For the CKM matrix elements, we adopt the Wolfenstein parameterization [81] and keep terms up to $\mathcal{O}(\lambda^4)$:

$$V_{ud} = 1 - \frac{1}{2}\lambda^2 - \frac{1}{8}\lambda^4 + \mathcal{O}(\lambda^6), \quad V_{us} = \lambda + \mathcal{O}(\lambda^7), \quad V_{cb} = A\lambda^2 + \mathcal{O}(\lambda^8), \quad (\text{B1})$$

with the inputs $A = 0.811 \pm 0.026$ and $\lambda = 0.22506 \pm 0.00050$ [65].

The hadronic inputs are summarized as follows: the pole masses of quarks are [65]

$$\begin{aligned} m_u = m_d = m_s = 0, \quad m_c = 1.67 \pm 0.07 \text{ GeV}, \\ m_b = 4.78 \pm 0.06 \text{ GeV}, \quad m_t = 174.2 \pm 1.4 \text{ GeV}; \end{aligned} \quad (\text{B2})$$

In the evaluation of Wilson coefficients $C_i(\mu)$ [52], the following inputs [65],

$$\begin{aligned} \alpha_s(M_Z) = 0.1182 \pm 0.0012, \quad \sin^2 \theta_W = 0.2313, \\ M_Z = 91.1876 \text{ GeV}, \quad M_W = 80.385 \text{ GeV}, \end{aligned} \quad (\text{B3})$$

are used. For the decay constants of light mesons, we take the results given in Ref. [82], which are an update of the ones extracted in Ref. [83]; for the decay constant of B_c meson, we adopt the results based on the lattice QCD [84]. Their values are

$$\begin{aligned} f_\rho = 215 \pm 6 \text{ MeV}, \quad f_\rho^\perp(2 \text{ GeV})/f_\rho = 0.70 \pm 0.04, \\ f_{K^*} = 209 \pm 7 \text{ MeV}, \quad f_{K^*}^\perp(2 \text{ GeV})/f_{K^*} = 0.73 \pm 0.04, \\ f_\omega = 188 \pm 10 \text{ MeV}, \quad f_\omega^\perp(2 \text{ GeV})/f_\omega = 0.70 \pm 0.10, \\ f_\phi = 229 \pm 3 \text{ MeV}, \quad f_\phi^\perp(2 \text{ GeV})/f_\phi = 0.750 \pm 0.020 \\ f_{B_c} = 487 \pm 5 \text{ MeV}, \end{aligned} \quad (\text{B4})$$

in which, the scale dependence of the transverse decay constants is taken into account via the leading-logarithmic running $f_\perp(\mu) = f_\perp(\mu_0) [\alpha_s(\mu)/\alpha_s(\mu_0)]^{4/23}$ [83]. For the renormalization scale, we take $\mu = m_{B_c}/2$ as default input, and vary it in the range $[m_{B_c}/2, m_{B_c}]$ to assess the scale uncertainty.

For the other well-determined inputs, such as the masses and lifetimes of mesons and Fermi constant *etc.*, we take their central values given by PDG [65]. In addition, the values of specific parameters, Λ_h in scheme I and m_g in scheme II, are given and discussed in the text.

Appendix C: Aguilar-Paparrassiliou's prescription

Besides Cornwall's prescription, Aguilar and Paparrassiliou also show a massive propagator effectively describing the solution of the Schwinger-Dyson equation with two possible behaviors at large q^2 [78]. One is similar to Eq. (17), with logarithmic running $m_g(q^2) \propto \ln(q^2)^{-\gamma}$ [78]. The second power-law solution has the form

$$m^2(q^2) = \frac{m_0^4}{q^2 + m_0^2} \left[\ln \left(\frac{q^2 + \rho m_0^2}{\Lambda^2} \right) / \ln \left(\frac{\rho m_0^2}{\Lambda^2} \right) \right]^{\gamma_2 - 1}, \quad (\text{C1})$$

which is used in the evaluation to compare with the results based on the Cornwall's prescription. The running coupling constant is given by

$$g^2(q^2) = \left[b \ln \left(\frac{q^2 + f(q^2, m^2(q^2))}{\Lambda^2} \right) \right]^{-1}, \quad (\text{C2})$$

where the function $f(q^2, m^2(q^2))$ is given by a power law expression

$$f(q^2, m^2(q^2)) = \rho_1 m^2(q^2) + \rho_2 \frac{m^4(q^2)}{q^2 + m^2(q^2)} + \rho_3 \frac{m^6(q^2)}{[q^2 + m^2(q^2)]^2}, \quad (\text{C3})$$

with $b = 33/48\pi^2$. The values of parameters $\rho = 1.046$, $m_0^2 = 0.5\text{GeV}^2$, $\Lambda = 0.3\text{GeV}$, $\gamma_2 = 2.12$, $\rho_1 = 1.205$, $\rho_2 = -0.690$, $\rho_3 = 0.121$ are suggested in Ref. [78]. One may refer to Refs. [66, 78] for detail for this part.

Acknowledgements

This work is supported by the National Natural Science Foundation of China (Grant Nos. 11475055, 11547014 and 11275057). Q. Chang is also supported by the Foundation for the Author of National Excellent Doctoral Dissertation of China (Grant No. 201317), the Program for Science and Technology Innovation Talents in Universities of Henan Province (Grant No. 14HASTIT036), the Excellent Youth Foundation of HNNU and the CSC (Grant

-
- [1] C. H. Chang and Y. Q. Chen, Phys. Rev. D **49**, 3399 (1994).
 - [2] N. Brambilla *et al.* [Quarkonium Working Group Collaboration], hep-ph/0412158.
 - [3] N. Brambilla *et al.*, Eur. Phys. J. C **71**, 1534 (2011).
 - [4] F. Abe *et al.* [CDF Collaboration], Phys. Rev. Lett. **81**, 2432 (1998).
 - [5] I. P. Gouz, V. V. Kiselev, A. K. Likhoded, V. I. Romanovsky and O. P. Yushchenko, Phys. Atom. Nucl. **67**, 1559 (2004) [Yad. Fiz. **67**, 1581 (2004)].
 - [6] R. Aaij *et al.* [LHCb Collaboration], Phys. Rev. D **87**, no. 11, 112012 (2013) Addendum: [Phys. Rev. D **89**, no. 1, 019901 (2014)].
 - [7] R. Aaij *et al.* [LHCb Collaboration], Phys. Lett. B **742**, 29 (2015).
 - [8] R. Aaij *et al.* [LHCb Collaboration], Phys. Rev. Lett. **108**, 251802 (2012).
 - [9] R. Aaij *et al.* [LHCb Collaboration], Phys. Rev. D **87**, 071103 (2013).
 - [10] R. Aaij *et al.* [LHCb Collaboration], JHEP **1309**, 075 (2013).
 - [11] R. Aaij *et al.* [LHCb Collaboration], JHEP **1311**, 094 (2013).
 - [12] R. Aaij *et al.* [LHCb Collaboration], Phys. Rev. Lett. **118** (2017) no.11, 111803.
 - [13] R. Aaij *et al.* [LHCb Collaboration], Phys. Rev. Lett. **111**, no. 18, 181801 (2013).
 - [14] R. Aaij *et al.* [LHCb Collaboration], Phys. Lett. B **759**, 313 (2016).
 - [15] I. I. Y. Bigi, Phys. Lett. B **371**, 105 (1996).
 - [16] M. Beneke and G. Buchalla, Phys. Rev. D **53**, 4991 (1996).
 - [17] V. V. Kiselev, J. Phys. G **30**, 1445 (2004).
 - [18] V. V. Kiselev, A. E. Kovalsky and A. K. Likhoded, Nucl. Phys. B **585**, 353 (2000).
 - [19] G. T. Bodwin, E. Braaten and G. P. Lepage, Phys. Rev. D **51**, 1125 (1995) Erratum: [Phys. Rev. D **55**, 5853 (1997)].
 - [20] D. S. Du, G. R. Lu and Y. D. Yang, Phys. Lett. B **387**, 187 (1996).
 - [21] Y. L. Yang, J. F. Sun and N. Wang, Phys. Rev. D **81**, 074012 (2010).
 - [22] J. Sun, Y. Yang, Q. Chang and G. Lu, Phys. Rev. D **89**, no. 11, 114019 (2014).
 - [23] J. Sun, Y. Yang and G. Lu, Sci. China Phys. Mech. Astron. **57**, no. 10, 1891 (2014).
 - [24] X. Liu, Z. J. Xiao and C. D. Lu, Phys. Rev. D **81**, 014022 (2010).
 - [25] Z. Rui, W. F. Wang, G. x. Wang, L. h. Song and C. D. Lv, Eur. Phys. J. C **75** (2015) no.6,

- [26] Z. Rui, H. Li, G. x. Wang and Y. Xiao, Eur. Phys. J. C **76** (2016) no.10, 564.
- [27] X. Liu and Z. J. Xiao, Phys. Rev. D **81** (2010) 074017.
- [28] X. Liu and Z. J. Xiao, Phys. Rev. D **82** (2010) 054029.
- [29] X. Liu and Z. J. Xiao, J. Phys. G **38** (2011) 035009.
- [30] Z. J. Xiao and X. Liu, Phys. Rev. D **84** (2011) 074033.
- [31] X. Liu, R. H. Li, Z. T. Zou and Z. J. Xiao, arXiv:1703.05982 [hep-ph].
- [32] J. Sun, N. Wang, Q. Chang and Y. Yang, Adv. High Energy Phys. **2015**, 104378 (2015).
- [33] S. Descotes-Genon, J. He, E. Kou and P. Robbe, Phys. Rev. D **80**, 114031 (2009).
- [34] N. Wang, Adv. High Energy Phys. **2016**, 6314675 (2016).
- [35] P. Colangelo and F. De Fazio, Phys. Rev. D **61**, 034012 (2000).
- [36] V. V. Kiselev, A. E. Kovalsky and A. I. Onishchenko, Phys. Rev. D **64**, 054009 (2001).
- [37] W. L. Ju, G. L. Wang, H. F. Fu, Z. H. Wang and Y. Li, JHEP **1509** (2015) 171.
- [38] C. Chang, H. F. Fu, G. L. Wang and J. M. Zhang, Sci. China Phys. Mech. Astron. **58** (2015) no.7, 071001.
- [39] M. Beneke, G. Buchalla, M. Neubert and C. T. Sachrajda, Phys. Rev. Lett. **83** (1999) 1914.
- [40] M. Beneke, G. Buchalla, M. Neubert and C. T. Sachrajda, Nucl. Phys. B **591** (2000) 313.
- [41] M. Beneke, G. Buchalla, M. Neubert and C. T. Sachrajda, Nucl. Phys. B **606**, 245 (2001).
- [42] M. Beneke and M. Neubert, Nucl. Phys. B **675** (2003) 333.
- [43] J. M. Cornwall, Phys. Rev. D **26**, 1453 (1982).
- [44] J. M. Cornwall and J. Papavassiliou, Phys. Rev. D **40** (1989) 3474.
- [45] J. Papavassiliou and J. M. Cornwall, Phys. Rev. D **44** (1991) 1285.
- [46] S. Bar-Shalom, G. Eilam and Y. D. Yang, Phys. Rev. D **67**, 014007 (2003).
- [47] Y. D. Yang, F. Su, G. R. Lu and H. J. Hao, Eur. Phys. J. C **44**, 243 (2005).
- [48] Q. Chang, X. Q. Li and Y. D. Yang, JHEP **0809**, 038 (2008).
- [49] Q. Chang, X. W. Cui, L. Han and Y. D. Yang, Phys. Rev. D **86**, 054016 (2012).
- [50] Q. Chang and Y. D. Yang, Nucl. Phys. B **852**, 539 (2011).
- [51] G. Buchalla, A. J. Buras and M. E. Lautenbacher, Rev. Mod. Phys. **68** (1996) 1125.
- [52] A. J. Buras, hep-ph/9806471.
- [53] M. Kobayashi and T. Maskawa, Prog. Theor. Phys. **49** (1973) 652.
- [54] G. P. Lepage and S. J. Brodsky, Phys. Rev. D **22** (1980) 2157.

- [55] M. Beneke, J. Rohrer and D. Yang, Nucl. Phys. B **774**, 64 (2007).
- [56] K. Wang and G. Zhu, Phys. Rev. D **88**, 014043 (2013).
- [57] Q. Chang, X. Hu, J. Sun and Y. Yang, Phys. Rev. D **91**, 074026 (2015).
- [58] Q. Chang, J. Sun, Y. Yang and X. Li, Phys. Lett. B **740**, 56 (2015).
- [59] Q. Chang, J. Sun, Y. Yang and X. Li, Phys. Rev. D **90**, no. 5, 054019 (2014).
- [60] G. Bell and T. Feldmann, JHEP **0804**, 061 (2008).
- [61] S. J. Brodsky and C. R. Ji, Phys. Rev. Lett. **55**, 2257 (1985).
- [62] P. Ball, V. M. Braun, Y. Koike and K. Tanaka, Nucl. Phys. B **529**, 323 (1998).
- [63] F. Su, Y. L. Wu, Y. D. Yang and C. Zhuang, Eur. Phys. J. C **48**, 401 (2006).
- [64] R. E. Cutkosky, J. Math. Phys. **1**, 429 (1960).
- [65] C. Patrignani *et al.* [Particle Data Group], Chin. Phys. C **40**, no. 10, 100001 (2016).
- [66] A. Deur, S. J. Brodsky and G. F. de Teramond, Prog. Part. Nucl. Phys. **90** (2016) 1.
- [67] A. C. Aguilar, A. A. Natale and P. S. Rodrigues da Silva, Phys. Rev. Lett. **90**, 152001 (2003).
- [68] D. Binosi, C. Mezrag, J. Papavassiliou, C. D. Roberts and J. Rodriguez-Quintero, arXiv:1612.04835 [nucl-th].
- [69] R. Aouane, F. Burger, E. M. Ilgenfritz, M. Müller-Preussker and A. Sternbeck, Phys. Rev. D **87**, 114502 (2013).
- [70] S. Gongyo and H. Suganuma, Phys. Rev. D **87**, 074506 (2013).
- [71] A. Deur, S. J. Brodsky and G. F. de Teramond, Phys. Lett. B **757** (2016) 275.
- [72] A. Courtoy and S. Liuti, Phys. Lett. B **726** (2013) 320.
- [73] C. R. Ji, A. F. Sill and R. M. Lombard, Phys. Rev. D **36** (1987) 165.
- [74] C. R. Ji and F. Amiri, Phys. Rev. D **42** (1990) 3764.
- [75] A. C. Aguilar, A. Mihara and A. A. Natale, Phys. Rev. D **65** (2002) 054011.
- [76] S. J. Brodsky, C. R. Ji, A. Pang and D. G. Robertson, Phys. Rev. D **57** (1998) 245.
- [77] K. G. Chetyrkin, B. A. Kniehl and M. Steinhauser, Phys. Rev. Lett. **79** (1997) 2184.
- [78] A. C. Aguilar and J. Papavassiliou, Eur. Phys. J. A **35**, 189 (2008)
- [79] C. D. Lu, K. Ukai and M. Z. Yang, Phys. Rev. D **63**, 074009 (2001)
- [80] M. Beneke and M. Neubert, Nucl. Phys. B **651**, 225 (2003).
- [81] L. Wolfenstein, Phys. Rev. Lett. **51**, 1945 (1983).
- [82] M. Jung, X. Q. Li and A. Pich, JHEP **1210**, 063 (2012).
- [83] P. Ball, G. W. Jones and R. Zwicky, Phys. Rev. D **75**, 054004 (2007).

[84] T. W. Chiu *et al.* [TWQCD Collaboration], Phys. Lett. B **651**, 171 (2007).